Clim Dyn
DOI 10.1007/s00382-012-1551-5

A multi-physics ensemble of regional climate change projections over the Iberian Peninsula

Sonia Jerez · Juan Pedro Montavez · Juan Jose Gomez-Navarro · Raquel Lorente-Plazas · Juan Andres Garcia-Valero · Pedro Jimenez-Guerrero

Received: 21 June 2012 / Accepted: 29 September 2012

Abstract This study illustrates the sensitivity of regional climate change projections to the model physics. A single-model (MM5) multi-physics ensemble of regional climate simulations over the Iberian Peninsula for present (1970–1999) and future (2070–2099 under the A2 scenario) periods is assessed. The ensemble comprises eight members resulting from the combination of two options of parameterization schemes for the planetary boundary layer, cumulus and microphysics. All the considered combinations were previously evaluated by comparing hindcasted simulations to observations, none of them providing clearly outlying climates. Thus, the differences among the various ensemble members (spread) in the future projections could be considered as a matter of uncertainty in the change signals (as similarly assumed in multi-model studies). The results highlight the great dependence of the spread on the synoptic conditions driving the regional model. In particular, the spread generally amplifies under the future scenario leading to a large spread accompanying the mean change signals, as large as the magnitude of the mean projected changes and analogous to the spread obtained in multi-model ensembles. Moreover, the sign of the projected change varies depending on the choice of the model physics in many cases. This, together with the fact that the key mechanisms identified for the simulation of the climatology of a given period (either present or future) and those introducing the largest spread in the projected changes differ significantly, make further claims for efforts to better understand and model the parameterized subgrid processes.

Keywords Parameterization schemes · Physics ensemble · Regional climate change projections · Iberian Peninsula

S. Jerez · J. P. Montavez (✉) · J. J. Gomez-Navarro · R. Lorente-Plazas · J. A. Garcia-Valero · P. Jimenez-Guerrero
Departmento de Fisica, Universidad de Murcia, Murcia, Spain
e-mail: montavez@um.es

S. Jerez
e-mail: sonia.jerez@gmail.com

J. J. Gomez-Navarro
e-mail: jjgomeznavarro@um.es

R. Lorente-Plazas
e-mail: lorente.plazas@gmail.com

J. A. Garcia-Valero
e-mail: jugarciav@aemet.es

P. Jimenez-Guerrero
e-mail: pedro.jimenezguerrero@um.es

S. Jerez
IDL, Universidade de Lisboa, Lisbon, Portugal

J. A. Garcia-Valero
Agencia Estatal de Meteorologia (AEMET), Murcia, Spain

1 Introduction

The western sector of the Mediterranean basin has been highlighted as a major climate change "hot-spot" (Giorgi 2006). In particular, the Iberian Peninsula (IP) shows significant changes at the end of this century in many climatic diagnostics, namely increased mean temperature and temperature variability, more frequent and intense heat waves and dry spells, and enhanced uneven heavy precipitation events (Perez et al. 2010; Gomez-Navarro et al. 2010; Jerez et al. 2012a). These climate change-related assessments for the IP are usually based on Regional Climate Models (RCMs) simulations shaping the large-scale signals according to the regional and local characteristics by

Published online: 12 October 2012

dynamically downscaling coarser databases obtained with Global Circulation Models (GCMs). Although the resolution of the GCMs has increased impressively in recent years, they are still hard able to capture accurately the large heterogeneity of the IP, where the added value of the RCMs is essential (Herrera et al. 2010; Argüeso et al. 2011; Gomez-Navarro et al. 2011; Soares et al. 2012).

A cascade of uncertainties befalls inevitably during such a downscaling process. The first and likely the most important source of uncertainty when projecting future changes derives from the assumptions about the future radiative scenario (IPCC 2007). The second is the fact that different GCMs, or different setups of the same GCM, provide different primary databases to be downscaled by RCMs (Gomez-Navarro et al. 2012). Last, the fact that different RCMs, or different setups of the same RCM, provide as well different results (Deque et al. 2007). In order to characterize, understand and reduce uncertainties, many research projects deal with ensembles of simulations obtained from different models and/or for different future scenarios, from which common signals and the accompanying spread, namely uncertainty (Tebaldi and Knutti 2007), can be identified (e.g. Deque et al. 2007; Haugen and Iversen 2008; Gomez-Navarro et al. 2010; Joshi et al. 2011). However, to the best of our knowledge there is a lack of studies focusing explicitly on the differences associated with the setup of RCMs regarding climate change projections (Knutson and Tuleya 2004; Seneviratne et al. 2006; Jerez et al. 2012a constitute the few distant precedents).

The setup of a RCM involves several aspects: the domains design, the nesting and nudging options, the execution strategy and, in some cases, the election of the parameterization schemes that model the subgrid processes. The later aspect provides the focus of this study. The parameterization schemes contain the so-called model physics and have been identified as the most important components of the numerical prediction models (Stensrud 2007). Currently, there is a vast spectrum of parameterization schemes accounting for the same features available to be incorporated in the RCMs. They differ in the level of complexity, the assumptions and approximations made to reduce the huge dimension of the related physics problem, the approach followed to solve it, and the areas and applications for which they were primarily developed.

Several works are devoted to assess the performance of diverse parameterization schemes aimed at identifying the best options to be employed in subsequent work as well as the features of the schemes that either have yet to be improved or add clear accuracy (e.g. Ratnam and Kumar 2005; Fernandez et al. 2007; Han et al. 2008; Jerez et al. 2010; Argüeso et al. 2011; Evans et al. 2012; Gianotti et al. 2012). In a previous work, we explored the sensitivity of present-day regional climate simulations to the model physics when reproducing the climatology of the IP, mainly mean values and interannual variability of temperature and precipitation (Jerez et al. 2012b). For that we assessed an ensemble of hindcast simulations, each one performed with different parameterization schemes for modeling the Planetary Boundary Layer (PBL), the cumulus (CML) and the microphysical (MIC) processes (two parameterization options were considered for each) within the mesoscale model MM5 (Grell et al. 1994). The results displayed spreads among the various simulations of alike magnitude as the spreads obtained in similar multi-model ensembles of hindcasts (Jacob et al. 2007), hence proving the huge role played by the model physics. An original methodology was applied in order to isolate the best options, and, although some schemes showed a priori better performances, the analysis also revealed important exceptions supporting a better job of their counterparts. Moreover, none of the simulations provided clearly outlying climates. Therefore, the question about the most appropriate model physics still remains strictly unanswered, which is in agreement with the recent study by Argüeso et al. (2011).

Furthermore, although it is commonly assumed that the most accurate models and parameterization schemes for simulating the present-day climate will still constitute the best tools for simulating future climates (e.g. Sanchez et al. 2004; Leung and Gustafson 2005), it could happen that under different conditions (as they may be in the future) other approximations and modeling approaches to those performing best in present conditions hold better. This concern adds uncertainty in the last stage of the aforementioned process aimed at obtaining regional climate change projections. However it could occur that errors cancel when subtracting future minus present simulated climatologies (Liang et al. 2008). If this hypothesis works, the uncertainty derived from the a priori ignorance of the best tools to simulate the unknown future conditions would not be as relevant.

Under this umbrella, the main objective of this study is to extend the previous assessment by exploring the role of the model physics for regional climate change applications over the IP. There are several aspects addressed in this work, like the analysis of the dependence of the spread among simulations on the driving conditions of the RCM. The question of its change under future conditions is of special concern. This contribution also tries to define the mean change signals, the associated spread (checking whether it is comparable to the spread obtained in multi-model ensembles) and the processes determining it. Last we describe the relationships (if any) between present-day biases and future projections within the multi-physics ensemble. Sections 2 and 3 summarize the experiments performed and the methodology utilized, and Sects. 4, 5

and 6 present the results. Summary and conclusions are provided in Sect. 7.

2 Experimental design

This work assesses two sets of simulations spanning the periods 1970–1999, as a control reference period (CTRL), and 2070–2099, as a future enhanced green house gas and aerosol concentrations scenario (SCEN), respectively. The simulations were performed using a climate version of the regional model MM5 (Grell et al. 1994) driven by the ECHAM5-Run1 simulation (Roeckner et al. 2003) forced by the SRES-A2 scenario in the future period (Nakicenovic et al. 2000). MM5 has been used in many research works (e.g. Jung and Kunstmann 2007; Evans 2008, 2010; Koo et al. 2009; Gomez-Navarro et al. 2010; Jerez et al. 2010, 2012a) and its ability to reproduce regional circulations and mesoscale climatological features has been widely proved (Kanamitsu et al. 2002; Evans et al. 2004; Gomez-Navarro et al. 2011). This, together with the fact that it has a wide spectrum of physics options, makes MM5 a suitable tool for assessing the role of the parameterization schemes when projecting future climate changes at regional scales.

Each set of simulations consists of a multi-physics ensemble comprising eight members resulting from varying the physical configuration of MM5 as follows. For the PBL scheme, we use either the MRF (Hong and Pan 1996) or the Eta (Janjic 1994) model; for the CML scheme, we use either the Grell (GR; Grell 1993) or the Kain-Fritsch (KF; Kain and Fritsch 1990) model; and for the MIC scheme, we use either the Simple Ice (SI; Dudhia 1989) or the Mixed Phase (MP; Reisner et al. 1998) model. Table 1 shows the configuration of schemes used in each member of the ensemble. A detailed description of the formulations and performances of these schemes can be found in Jerez et al. (2012b). Both schemes in each case meet two criteria: (1) both have proven skill and are, therefore, commonly used, and (2) both are based on very different physical approaches. This motivated our election.

Table 1 Combination of the PBL, CML and MIC schemes used in each simulation of the multi-physics ensemble

Sim.	PBL	CML	MIC
1	Eta	GR	SI
2	MRF	GR	SI
3	Eta	KF	SI
4	MRF	KF	SI
5	Eta	GR	MP
6	MRF	GR	MP
7	Eta	KF	MP
8	MRF	KF	MP

The rest of the MM5 physics options were fixed and are common in all the simulations. For the radiation processes we use the RRTM option (Mlawer et al. 1997); particularly a home-adapted version of it that permits the inclusion of the same radiative forcings in the regional simulation as those employed in the GCM run driving MM5. For the land-surface processes and land-atmosphere interactions we use the Noah Land-Surface Model (Chen and Dudhia 2001) which clearly enlarges the accuracy of the simulations in comparison to other options as it takes into account soil moisture-atmosphere interactions (Jerez et al. 2010).

The spatial configuration for the model runs consists of two two-way nested domains with resolutions of 90 km in the outer domain (D1) and 30 km in the inner domain (D2), as described in Jerez et al. (2012b). The latter covers the whole IP even after removing the blending area (first five cells from the borders). The outer domain was elongated eastward in order to take into account the strong influence that the Mediterranean Sea exerts over the IP (Font-Tullot 2000). Vertically, 24 unevenly spaced sigma-levels up to 100 hPa were considered.

The simulations were performed by splitting the whole 30-year long periods into subperiods of 5-year length that were then integrated by continuous runs with a spin-up period of 4 months that prevents both noisy outputs during the model stabilization (Giorgi and Bi 2000) and errors from a possible poor initialization of, specially, soil variables (Christensen 1999). All the runs were initialized using the ECHAM5 simulation providing the boundary conditions except for the soil moisture variable. Soil moisture was initialized, and not updated at the boundaries afterward, in in each re-initialization, either of the present or the future period, using a summer climatology (all the runs start on September the 1st) obtained from reanalysis data. This provides not extreme but 'realistic' initialization of this strongly inertial variable that the model can easily adjust during the spin-up period. Every 6 h (at 00, 06, 12 and 18 h of each day) the MM5 outputs were recorded and the boundary conditions from the GCM simulation were updated (without nudging). This experimental design optimizes our computational resources (Jerez et al. 2009), prevents that the regional model drifts so much from the driving conditions during the course of long integrations (Lo et al. 2008) and has been used in several previous works (e.g. Gomez-Navarro et al. 2010; Jerez et al. 2012a). The non-existence of artificial 5-years cycles in our simulations has been specifically checked.

3 Methodology

The analysis focuses on seasonal averages of 2-m temperature (T) and precipitation (P). Both mean values and

interannual variability are assessed; the latter defined as the standard deviation (sdev) of the detrended seasonal series. Seasonal averages of daily maximum and minimum temperatures (TX and TN, respectively) have been also eventually investigated, as well as the intensity and frequency of the precipitation events (PI and PF, respectively). We define PF as the mean number of days within each season with precipitation above 1 mm, expressed in percentage, and PI as the mean precipitation amount in those rainy days.

We analyze the role of the model physics in both (1) present and future periods separately, and (2) projected changes (i.e. future-minus-present). For that we use a similar approach to that proposed in Jerez et al. (2012b), i.e. using the following statistics and concepts [which are explicitly described in Jerez et al (2012b)]:

- Ensemble mean (*EM*): mean value computed from all the values provided by every single member of the ensemble.
- Ensemble spread (*ES*): maximum difference among the various ensemble members.
- Mean ensemble spread (*MES*): sum of the PBL_{spread}, the CML_{spread} and the MIC_{spread}. These latter are called schemes-induced spreads and are defined as the difference, in absolute value, between the two ensemble means corresponding to the two 4-members subensembles that result from fixing each one of the two options for each parameterized process.
- Spread-controlling scheme or leading parameterized process (*LP*): the scheme whose change provokes the largest differences among simulations, i.e. the largest scheme-induced spread.

A statistical significance test is applied to the calculation of differences (in particular in Figs. 1, 9, 10, 11) so that they will be considered only if significant above the 95 % level. We apply a two-tailed *T* test to check the significance of differences in mean values and a two-tailed *F* test to check the significance of differences in sdev (Snedecor and Cochran 1989).

In order to account for the relative importance of spreads we compute the signal-to-noise ratio, defined as the ratio between the *ES* and the standard deviation of the *EM* series, as in Jerez et al. (2012b). A signal-to-noise ratio over 1 regarding mean values indicates that the *ES* in mean values exceeds one standard deviation of the *EM* series. A signal-to-noise ratio over 0.2 regarding sdev means that the *ES* in sdev represents over a 20 % of the sdev of the *EM* series. Both features have been highlighted in Figs. 3, 4, 6 and 7. Further, the *ES* in the projected changes is shown in percentage with respect to the mean change signals in Fig. 10 in order to measure its actual relevance.

4 Validation of the present-day simulations: GCM induced errors

In order to validate present-day regional climate simulations driven by GCMs runs aimed at being a reference when projecting future changes, a common procedure consists of contrasting them with analogous simulations driven by reanalysis data (Galos et al. 2007; Leander and Buishand 2007; Gomez-Navarro et al. 2011). Since large-scale climate errors in the global models are retained by the higher-spatial-resolution regional models (Rummukainen 2010), and given that reanalysis data can be considered as a surrogate of reality (Christensen et al. 1997; Salzmann et al. 2007), this procedure allows direct evaluation of the GCM induced errors. The RCM (MM5)-induced errors were already evaluated by direct comparison between hindcasted simulations and observations in the precedent paper by Jerez et al. (2012b). In such assessment the highlighted MM5-weaknesses were mainly related to a systematic underestimation of Tmean, poor reproduction of the Tsdev patterns, and overprediction (underprediction) of the light (heavy) rainfall; being Pmean and Psdev closely related.

This section describes the comparison between the CTRL *EM* and the HNDC *EM*. CTRL refers to the ensemble of control ECHAM5-driven simulations, while HNDC refers to an analogous ensemble of hindcast simulations reported in Jerez et al. (2012b). Both ensembles consist of the same members, have identical model setups, and span the same period, with the only difference being the driving conditions. Figure 1 shows the CTRL *EM* climatologies and their difference with respect to the HNDC *EM* climatologies. Both patterns (from the CTRL *EM* and from the HNDC *EM*) for each magnitude (Tmean, Tsdev, Pmean and Psdev) and for every season are also compared in the Taylor diagrams of Fig. 2.

CTRL simulations are colder than the HNDC simulations in most of the IP, which adds inaccuracy to the MM5-related cold bias already detected in Jerez et al. (2012b), except for the area around the Strait of Gibraltar where the CTRL simulations are warmer than the hindcasts in summer and autumn (Fig. 1a–d). The largest differences appear in these seasons, being up to 3 K. In spite of that, the spatial distribution and the spatial variability of the Tmean patterns is quite similar in both experiments, as the spatial correlation between the CTRL and the HNDC patterns is over 0.9 and the standard deviation ratio is just slightly over 1 (Fig. 2a).

The agreement between CTRL and HNDC simulations regarding Tsdev is smaller but still acceptable: the spatial correlation between the CTRL and the HNDC patterns is almost 0.6 in spring and around 0.8 in the rest of seasons, and the spatial variability is underestimated mainly in summer and autumn, with the standard deviation ratio around 0.6 and 0.8 respectively (Fig. 2b). Tsdev is

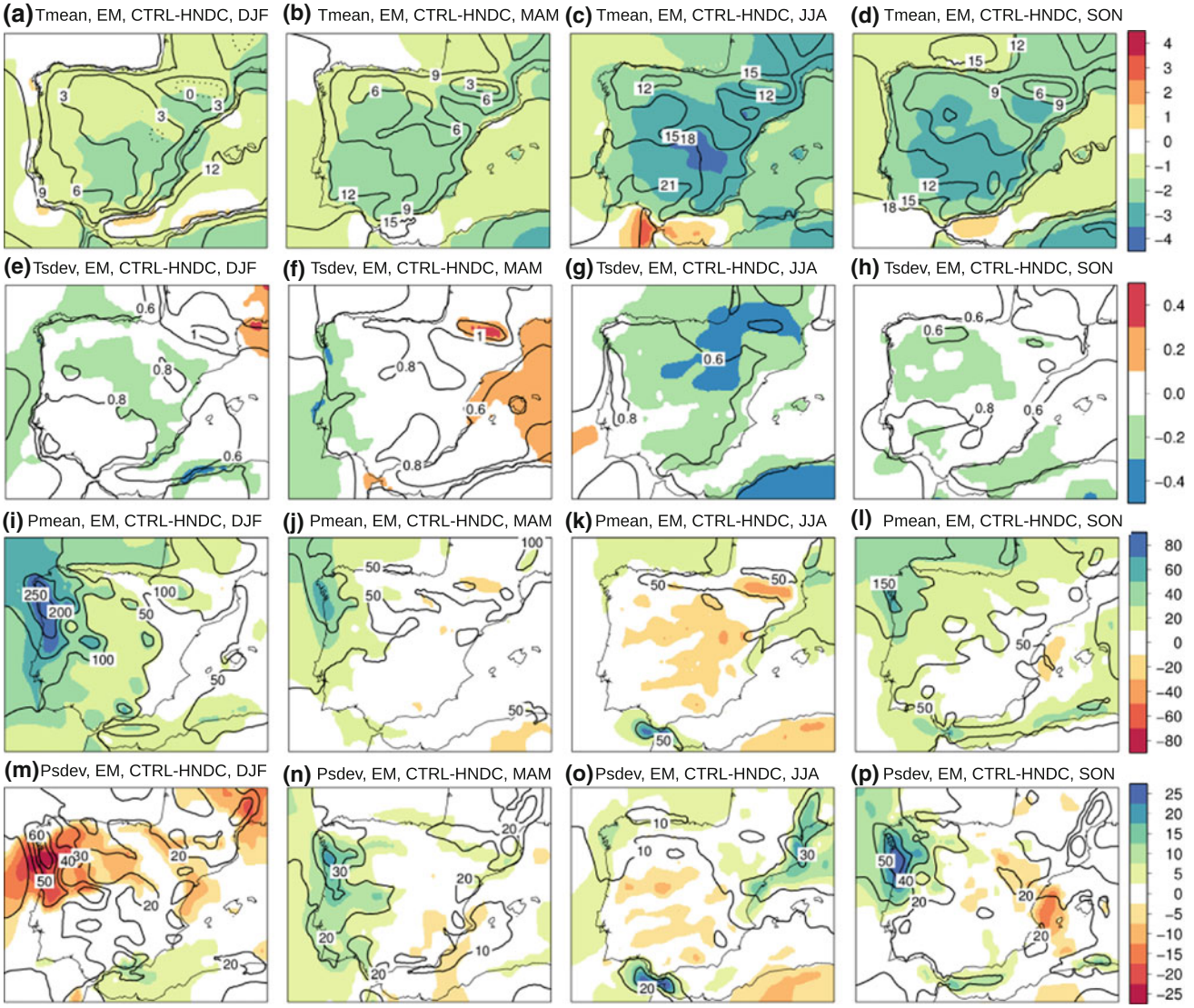

Fig. 1 CTRL ensemble mean (contour) and the difference with the HNDC ensemble mean (CTRL minus HNDC; *shaded*) for Tmean (*first row*), Tsdev (*second row*), Pmean (*third row*) and Psdev (*fourth row*). Differences are displayed only if they are statistically significant at the 95 % confidence level. Each column, from *left* to *right*, represents the winter, spring, summer and autumn seasons. Units: K for temperature (except contours in panels **a**–**d** which are in °*C*), and mm/month for precipitation

generally underestimated in the CTRL simulations when compared to the HNDC simulations, up to 0.4 K in the summer season (around 40 %), although a converse behavior appears in spring in the Pyrenees and over the Mediterranean Sea (Fig. 1e–h). It should be stressed that the agreement between CTRL and HNDC simulations is better than between HNDC and observations (Jerez et al. 2012b), and thus the main problem when simulating Tsdev should be attributed to the MM5 performance rather than to GCM inaccuracies.

The comparison of the Pmean patterns reveals that the CTRL simulations tend to overestimate the heavy amounts of precipitation (in winter and transitional seasons in western and northern areas, by up to 80 mm/month, i.e. around 60 %) and to underestimate the light rainfall (in summer in almost the whole IP, by up to 40 mm/month, i.e. also around 60 %) in comparison to the HNDC simulations (Fig. 1i–l). These differences show an opposite sign to the biases obtained when comparing the HNDC simulations with observations (Jerez et al. 2012b), but are around twice in magnitude. Therefore, where the hindcasted simulations were found to overestimate precipitation, the CTRL simulations underestimate it, and vice versa. The spatial correlation between the CTRL and the HNDC patterns of Pmean is above 0.7, increasing to 0.95 in the winter season. The spatial variability of the patterns is overestimated in the CTRL simulations, except in the summer season when it is well captured (Fig. 2c).

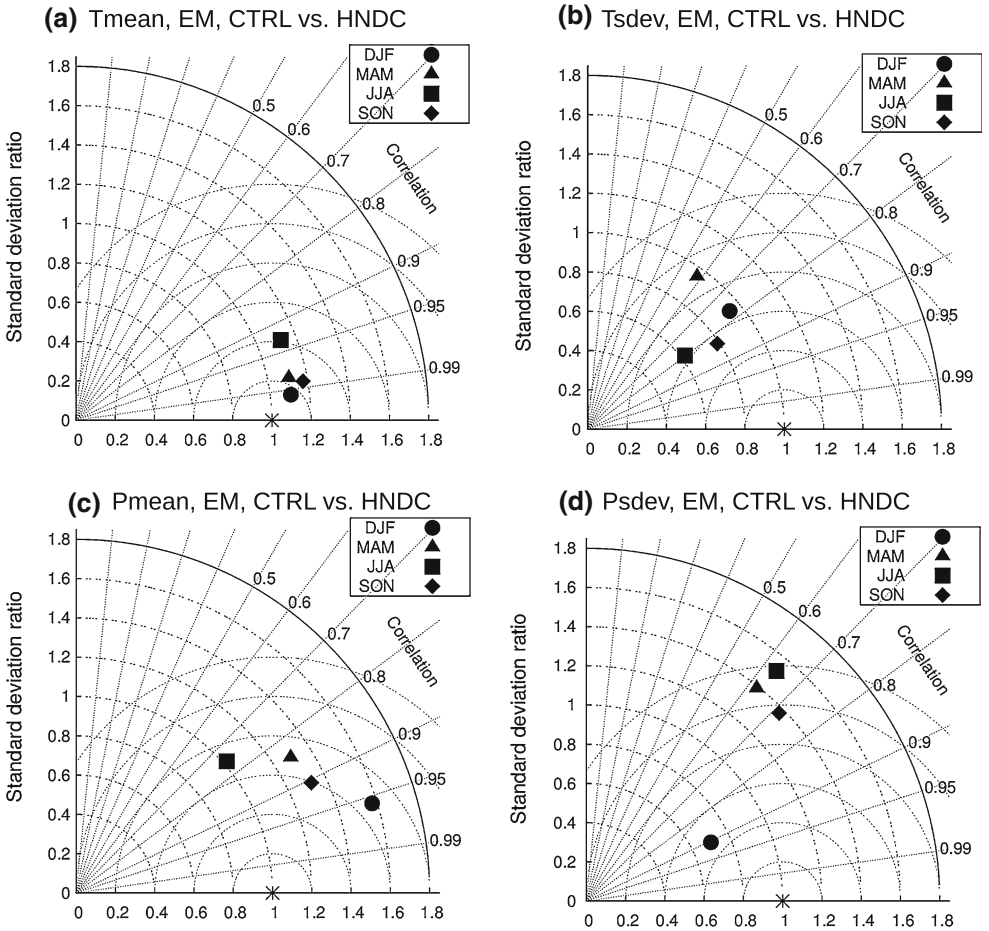

Fig. 2 Taylor diagrams comparing the CTRL ensemble mean seasonal patterns of **a** Tmean, **b** Tsdev, **c** Pmean and **d** Psdev with those corresponding to the HNDC ensemble mean

Regarding the standard deviation of the precipitation series (Fig. 1m–p), an overestimation/underestimation is generally found coinciding with the areas/seasons with overestimated/underestimated Pmean. However, although the CTRL simulations tend to produce more precipitation than the HNDC simulations over western areas in winter, the simulated interannual variability of precipitation is lower in the CTRL simulations than in the HNDC simulations there. This striking feature breaks the expected monotonous relationship between Pmean and Psdev. The largest errors are above 20 mm/month, which represents in some cases almost the 100 % of the HNDC simulated values. The Taylor diagram (Fig. 2d) shows that the spatial correlation between the CTRL and the HNDC patterns of Psdev is around 0.6–0.7 (growing to 0.9 in winter) and the spatial variability of the CTRL Psdev patterns is overall overestimated in comparison to the HNDC experiment (except in winter when it is underestimated).

Summarizing, the ECHAM5-Run1 conditions fosters the cold bias already detected in the hindcasted simulations and reduce the simulated interannual variability of the temperature series, but provides quite reliable boundary conditions for simulating the spatial patterns of both Tmean and Tsdev. Regarding the simulation of precipitation, meanwhile MM5 (in the hindcast mode) tends to overpredict/underpredict the light/heavy rainfall, the opposite is the case when it is driven by the ECHAM5-Run1. This implies an overall overestimation of the spatial variability of the Psdev and Pmean patterns, while a still acceptable reproduction of their spatial distribution. In general, the mean values are less dependent on the driving conditions than the interannual variability of the temperature and precipitation series.

This objective assessment provides enough confidence on the CTRL simulations, while highlights specific deficiencies that should be kept in mind. Moreover, these results constitute a valuable reference for future works.

5 Spreads dependence on the driving conditions

In the previous work by Jerez et al. (2012b) a thorough assessment of the spreads derived from the various model physics setups in the HNDC experiments was presented.

In this section we explore how spreads change depending on the large-scale features driving the regional model. First, we assess the spreads in the CTRL ensemble and compare them to the spreads in the HNDC ensemble (Sect. 5.1). This analysis will allow evaluation of whether the spreads and the associated leading parameterized processes change just because of the different synoptic conditions. Second, we compare the spreads in the SCEN ensemble to the spreads in the CTRL ensemble (Sect. 5.2) in order to investigate how the spreads and *LPs* change under the future scenario, thus anticipating the impact of the model physics in the future projections, which will be assessed in the last Section.

5.1 CTRL versus HNDC

Figure 3 shows the *ES* patterns obtained in the CTRL ensemble, as well as the differences with the analogous *ES* patterns from the HNDC ensemble.

The CTRL ES in mean temperature shows the highest values in winter and summer, up to 3 K inland, with a clear continental shape in the summer season, and ranges between 1 and 2 K in spring and autumn showing a very homogeneous distribution (Fig. 3a–d). In all cases these values exceed one standard deviation of the temperature series. Small differences with the *ES* in the HNDC ensemble are observed, mainly concentrated in the summer

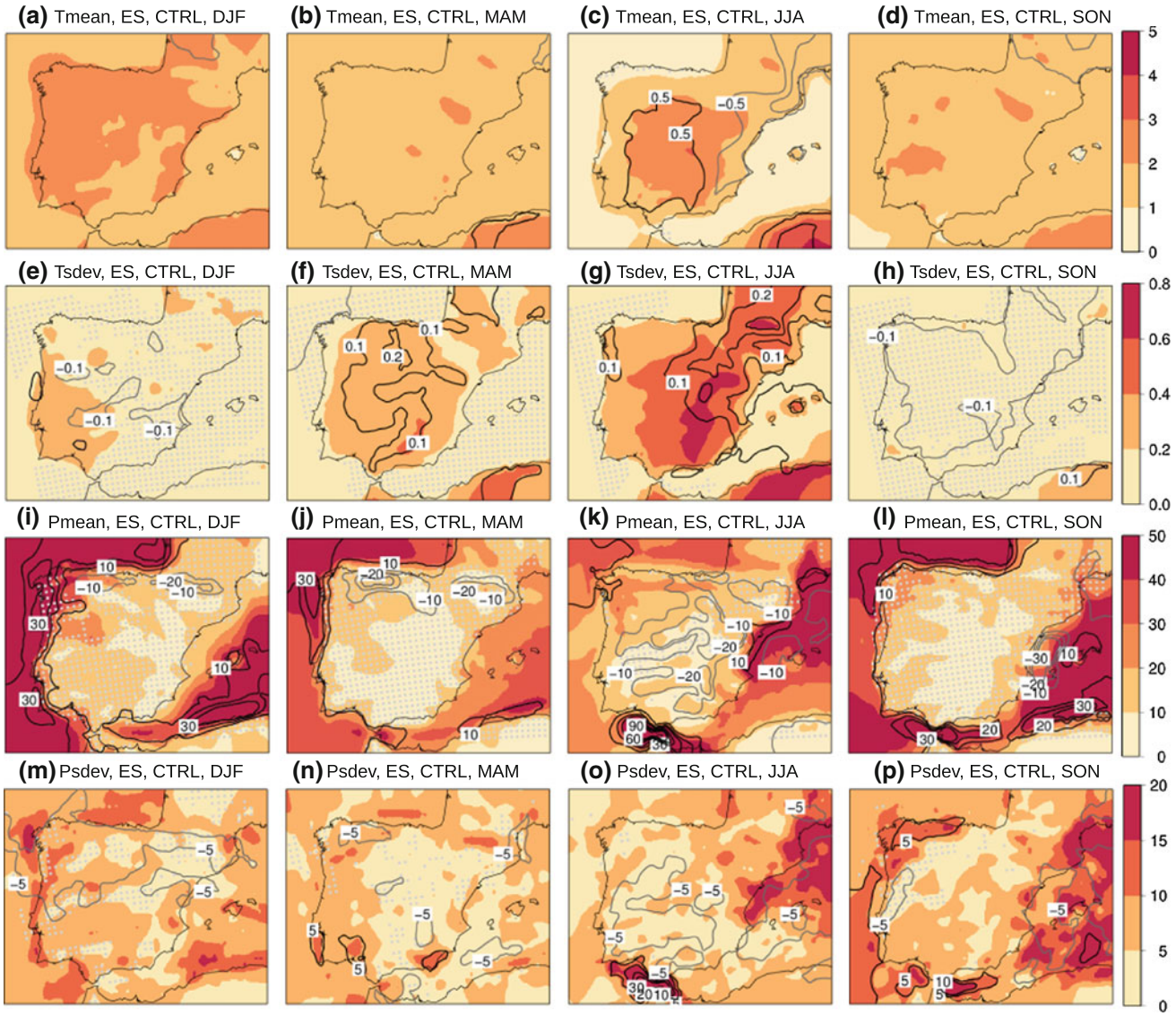

Fig. 3 CTRL ensemble spread (*shaded*; with the *gray dots* blurring the areas where the signal-to-noise ratio is below 1 in the case of Tmean and Pmean, and below 0.2, i.e. 20 %, in the case of Tsdev and Psdev) and the difference with the HNDC ensemble spread (CTRL minus HNDC; contours) for Tmean (*first row*), Tsdev (*second row*), Pmean (*third row*) and Psdev (*fourth row*). Each column, from *left* to *right*, represents the winter, spring, summer and autumn seasons. Units: K for temperature, and mm/month for precipitation

season when the CTRL *ES* is larger in the inner Iberia while smaller in the Mediterranean coast than the HNDC *ES* (differences are about 0.5 K).

The CTRL *ES* in Tsdev evolves from winter, with significant values mainly in southwestern Iberia (about 0.2–0.4 K, above the 20 % threshold in the signal-to-noise ratio), to summer, with differences up to 0.8 K among the various CTRL simulations in the inner eastern Iberia (which represents up to 80 % of the *EM* Tsdev values), exhibiting an intermediate pattern in spring and negligible *ES* values (below the 20 % threshold) in autumn in most of the IP (Fig. 3e–h). Differences with the HNDC *ES* are negative in winter and autumn (around −0.1 K), while positive and higher (up to 0.3 K) in spring and summer.

In the case of Pmean (Fig. 3i–l), the largest spreads, reaching above 50 mm/month, appear over the sea, being in general larger than in the HNDC ensemble (note the striking spread in the areas around the strait of Gibraltar) except for some areas in the Mediterranean shore. Inland, spreads implying a signal-to-noise ratio above 1 emerge only in the summer season, being up to 30 mm/month, depicting quite an orographic pattern and exhibiting smaller values (about half) than in the HNDC ensemble.

Large spreads appear in the assessment of Psdev, around 5–10 mm/month inland and 10–20 mm/month offshore, mainly in Mediterranean areas in summer and autumn, in most cases representing over 20 % of the *EM* Psdev values (Fig. 3m–p). In spite of that, they are still smaller than in the HNDC ensemble, with the exception of the areas around the strait of Gibraltar where, as for Pmean, huge spreads appear in the CTRL ensemble.

Therefore, the large spreads in the CTRL ensemble show a similar pattern but also important differences with the HNDC *ES* patterns provided by Jerez et al. (2012b), highlighting the dependence of the spreads on the driving conditions, i.e. the different performance of the various parameterization schemes under different synoptic conditions. On the other hand, it is worth noting that most of the outstanding areas in the error patterns of Fig. 1 show also large spreads (Fig. 3). Although nothing similar to a linear relationship between the error and the spread can be established, it is perceivable that there are areas showing a strong response to changes in both the synoptic forcing and the physical configuration of the model. This overlap suggests that the parameterized processes could be able to modify the synoptic conditions, which further emphasizes their crucial role. Hence, we would have both: the synoptic forcing determining the performance of the parameterization schemes and, at the same time, the parameterized processes modifying the synoptic circulation.

Next we explore which are the so-called leading parameterized processes (*LPs*) in the CTRL ensemble in order to elucidate if they also change with respect to the HNDC ensemble. Figure 4 depicts the *LPs* for each analyzed variable/statistic in the CTRL simulations, as well as its contribution to the mean ensemble spread (*MES*). We observe that (1) the PBL scheme determines the spread patterns for Tmean at every point and for Pmean over the sea, where the MRF scheme produces warmer and wetter conditions than the Eta model; (2) the CML scheme widely prevails in the Tsdev *MES* patterns of spring and summer, with the GR scheme providing larger values of Tsdev than the KF model, and in the Pmean *MES* pattern of summer (over land), where GR is drier than KF; and (3) the MIC scheme plays the major role regarding the simulated Tsdev in winter, with MP promoting larger values than SI. In the case of Psdev, there is no clear *LPs* over a wide region. These features appeared similarly in the HNDC ensemble (Jerez et al. 2012b). Thus, although the spread patterns look different in both ensembles, the leading parameterized processes are quite independent of the driving conditions.

Not only the leading parameterized processes and their comparative performances (i.e. the warmer, wetter, etc. schemes) are common in both ensembles, but also the relative performances of the individual ensemble members, ones with respect to the others. Figure 5 shows the deviations of the spatially averaged fields provided by each ensemble member of the CTRL ensemble with respect to the member 1, *versus* the same magnitude corresponding to the HNDC ensemble. Almost all the points in Fig. 5a, c, d concentrate close to the diagonal line, which means that differences in Tmean, Pmean and Psdev between the ensemble members are nearly constant in both ensembles. This result further reinforces the idea that the driving conditions provide the primary control over the forecasted magnitudes, while the physical configuration of the model mainly contributes to shape them. However, a striking feature arises in Fig. 5b: for Tsdev, the interactions between the parameterization schemes and the various synoptic forcings lead to a quite mixed diagram. This issue will be recalled and discussed later.

5.2 SCEN versus CTRL

This section further assesses the dependence of spreads on the driving conditions, now focusing particularly on how they show up under a future green house gases enhanced scenario. This study is primary based on Fig. 6 displaying the SCEN *ES* and its differences with the CTRL *ES*. The results show that, albeit the *ES* patterns show in both cases very similar structures, spreads are generally greater in the SCEN ensemble, up to twice in some cases. However, the *ES* in Tsdev diminishes in the future scenario, dropping below the 20 % threshold in all seasons but in summer.

In spite of the differences in the *ES* between both ensembles, the *LPs* do not change significantly in the SCEN ensemble but for Tsdev (Fig. 7). In this case, the CML predominance in spring and summer observed in the

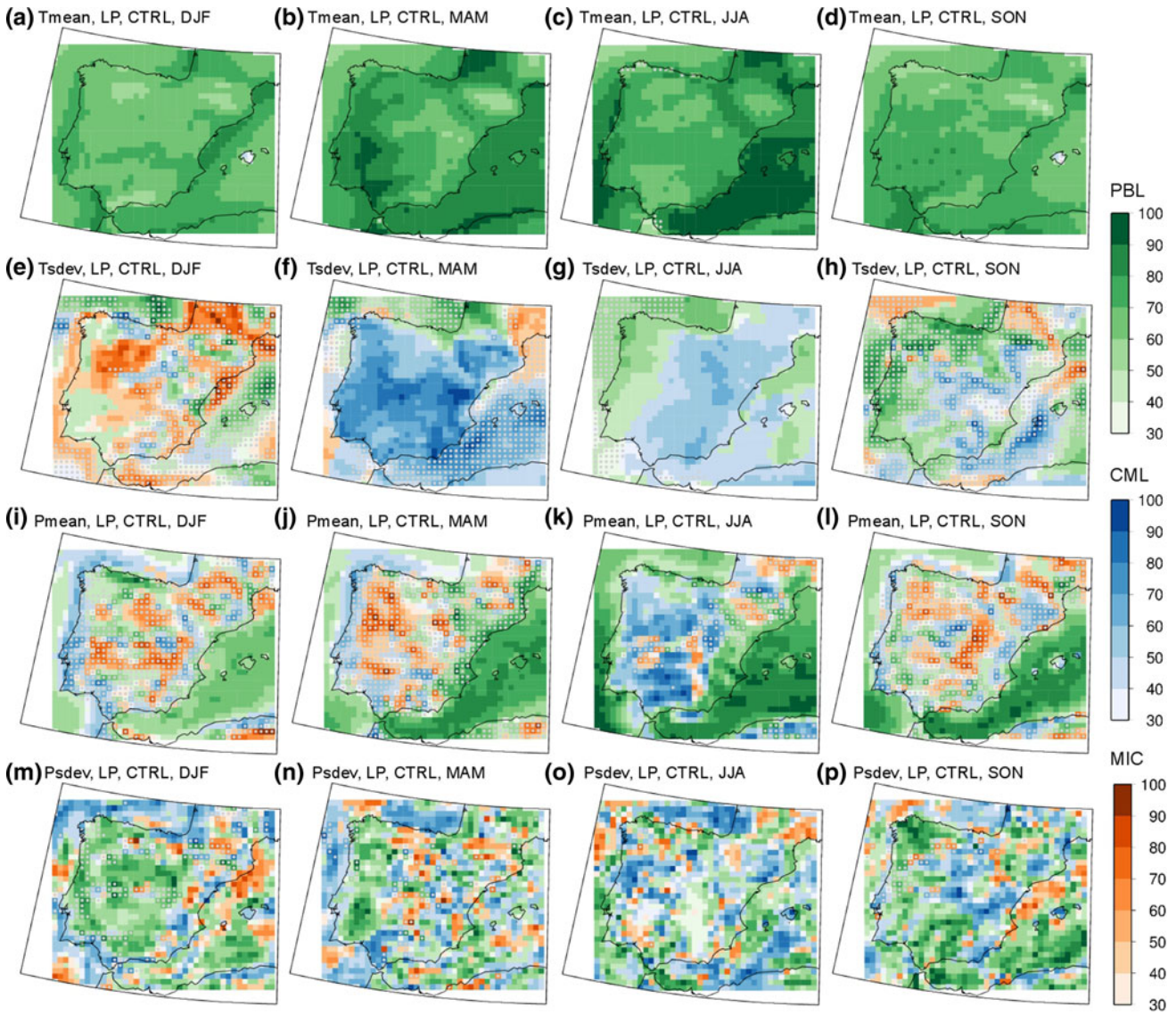

Fig. 4 Leading parameterized processes (*LPs*) for the simulated Tmean (*first row*), Tsdev (*second row*), Pmean (*third row*) and Psdev (*fourth row*) in the CTRL ensemble. The color indicates the *LP*: PBL (*green*), CML (*blue*) or MIC (*orange*). The intensity of the color represents the percentage of the mean ensemble spread (*MES*) due to the change of the *LP* scheme (units: %). The *gray dots* blur the areas where the signal-to-noise ratio is below 1 in the case of Tmean and Pmean, and below 0.2 (20 %) in the case of Tsdev and Psdev. Each column, from *left* to *right*, represents the winter, spring, summer and autumn seasons

CTRL ensemble disappears in the SCEN ensemble in favor of the PBL (Figs. 4f, g vs. 7f, g). But in general, the relative importance of some processes over the others remains also under the SCEN synoptic forcing. Moreover, Fig. 8 reveals that the relative response of the various ensemble members is similar in both the SCEN and the CTRL ensemble. Note that the case of Tsdev is also an exception here, as no order can be appreciated in Fig. 8b. In addition, Fig. 8b further shows that the range of variation among the diverse experiments in the simulated Tsdev is smaller in the SCEN than in the CTRL ensemble.

The results obtained for Tsdev suggest that an upper limit for the simulated Tsdev would be achieved in the future scenario, since all the simulations tend to converge within a small range in the SCEN ensemble while they disagree more widely in the CTRL ensemble. On the other hand, the change found for the *LPs* in the simulated Tsdev indicates that the processes controlling Tsdev in the present-period simulations lose relevance in the future scenario. After these findings, we recall the works by Seneviratne et al (2006), Jerez et al. (2010, 2012a) showing: (1) the main role played by the soil moisture for the simulation of Tsdev in the so-called transitional climate zones, i.e. those with intermediate regimes between dry and wet, as most of the IP can be currently classified, and (2) the severe drop in the soil moisture content projected for most of the IP at the end of this century

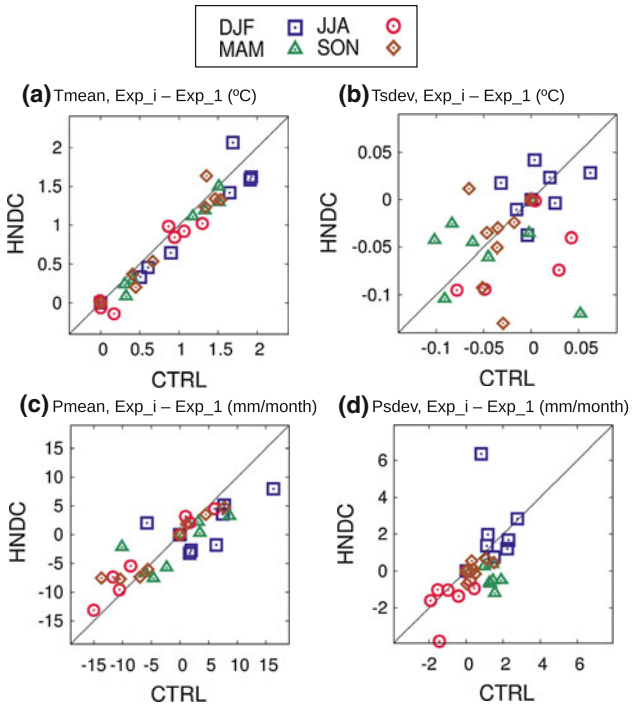

Fig. 5 CTRL versus HNDC comparison of spatially averaged fields from the seasonal patterns of **a** Tmean, **b** Tsdev, **c** Pmean and **d** Psdev obtained in each individual experiment of both ensembles. Each season is represented by one symbol and color (see legend). There are eight symbols per season corresponding to the eight ensemble members listed in Table 1. It is represented the difference between each experiment and the experiment 1 of Table 1

causing a strong northward shift of such a transitional climate zones and turning most of the IP into a dry regime. In those severe dry conditions, the role of the soil moisture in terms of variability becomes less relevant, implying a quasi-constant boundary condition for the simulation of Tsdev. These results would fit to some extent with our findings as follows: (1) the soil moisture content would control the simulation of Tsdev in the present period, when the different soil moisture content simulated by the various CTRL experiments is the primary reason that Tsdev differs among them, and (2) the severe drop in the soil moisture content in the future would give no space to the simulations to provide different results for Tsdev. However, since Pmean is the main contribution to the soil moisture content, this argument would require that the *LPs* for Tsdev and Pmean coincide in Fig. 4, but they do not. Hence, this hypothesis may work only partially and needs more research to be confirmed.

6 Change projections

6.1 Ensemble mean and spread

The role of the model physics in climate change projections is investigated in this section, supported by the results of the preceding section. Figures 9 and 10 display the *EM* signals of change and the spread associated. These results are computed in two ways, either from the absolute values of change (Fig. 9) or from the percentage values of change with respect to the CTRL climatologies (except for ΔTmean, Fig. 10). The black dots in these figures, in case, indicate that some ensemble members project increases while others decreases in the assessed magnitudes.

Based on the projections of the ensemble mean, both mean temperature and temperature variability are projected to increase, although the areas most affected in each case do not match. The *EM*-projections for mean temperature (Fig. 9a–d) show a clear annual cycle, with maxima in the summer season (up to 6 K in the south-west), minima in winter (around 3 K everywhere), and intermediate patterns in spring and autumn. Spreads follow a similar cycle being up to 3 K in summer, which represents up to 50 % of the ensemble mean-projected change, and decreasing to around 30–40 % in the rest of the seasons (Fig. 10a–d).

Regarding temperature variability (Figs. 9, 10e–h), the *EM*-projected changes are around 0.5 K (around 60–70 %) mainly affecting north-eastern areas in winter and summer and wide western regions in spring and autumn. Spreads are minimal in winter and autumn (0.2 K, 20 %, in small areas), grow in spring (0.2 K, 60 %) and soar in summer (up to 0.8 K, above 100 %), when they involve even disagreement in the sign of the change among the ensemble members over wide areas.

Projections for averaged maximum and minimum temperature (TX and TN) exhibit in both cases similar distribution and spreads as the projections for Tmean (not shown). Differences occur mainly in the intensity of the change signals, being in general higher for TX than for TN for both mean values and the standard deviation of the temperature series. However, the *EM*-projected change for TXsdev is smaller than for TNsdev in summer. This is because there is a great discrepancy regarding ΔTXsdev in summer among the ensemble members, with some projecting large increases while others considerable decreases that are canceled when averaging. This issue will be recalled below.

The ensemble mean projections foresees a general decrease in the amount of precipitation (Figs. 9, 10i–l) in spring and autumn (around 20–30 mm/month, around 30–40 % with a 10 % of spread) and in north-western Iberia in summer (around 10 mm/month, 30–50 % with a 20 % of spread). Conversely, small coastal areas of the Mediterranean and the region around the strait of Gibraltar show increases in mean precipitation in summer. Finally, no significant signals appear neither anywhere in winter nor in summer in the wide south-east. However, in summer, some of the areas with no significant signals exhibit large spreads (involving even disagreement in the sign of the change

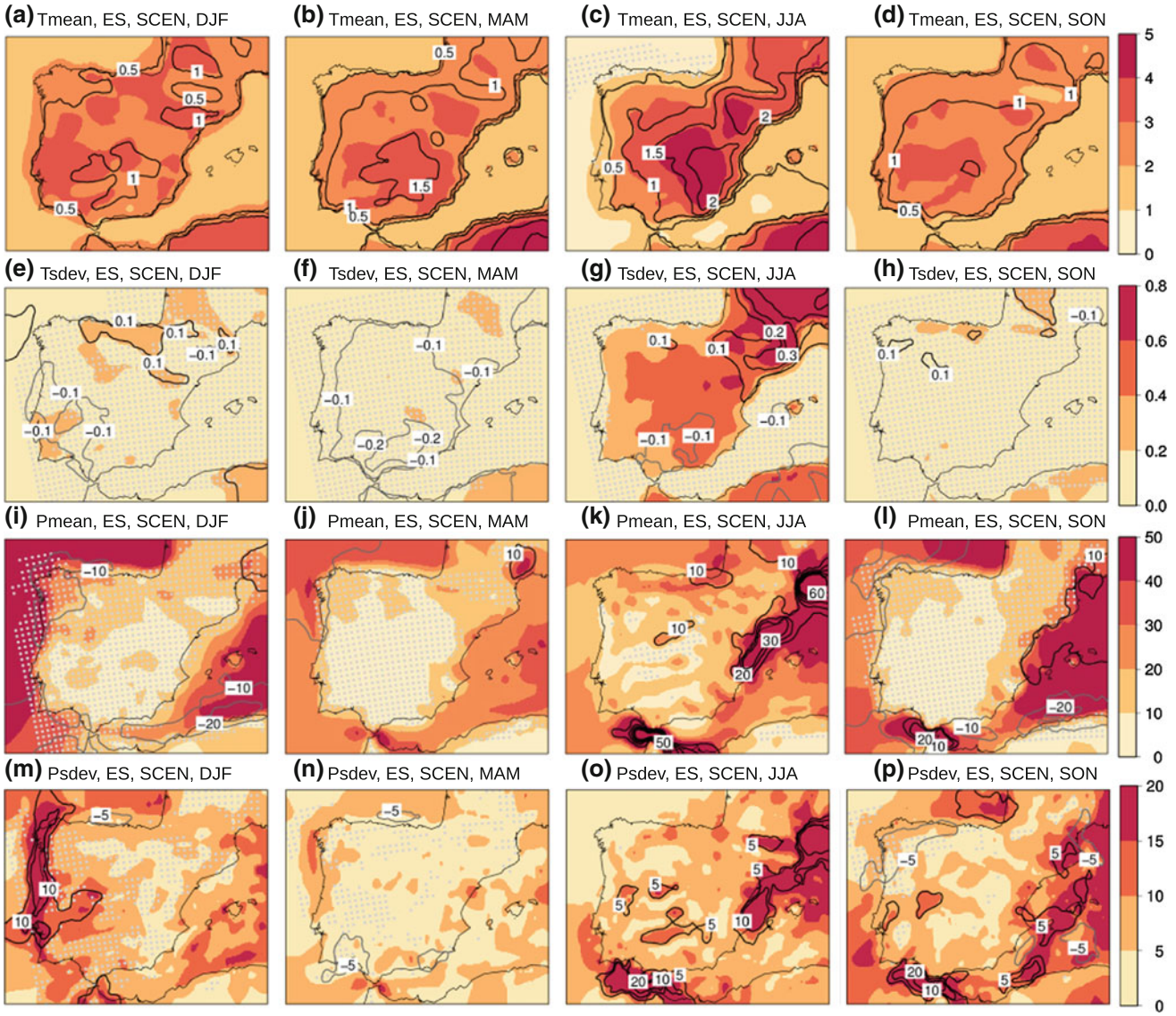

Fig. 6 (Analogous to Fig. 3). SCEN ensemble spread (*shaded*; with the *gray dots* blurring the areas where the signal-to-noise ratio is below 1 in the case of Tmean and Pmean, and below 0.2, i.e. 20 %, in the case of Tsdev and Psdev) and the difference with the CTRL ensemble spread (SCEN minus CTRL; contours) for Tmean (*first row*), Tsdev (*second row*), Pmean (*third row*) and Psdev (*fourth row*). Each column, from *left* to *right*, represents the winter, spring, summer and autumn seasons. Units: K for temperature, and mm/month for precipitation

among the ensemble members) such that nothing can be concluded. On the contrary, the spreads in winter are just around 10 %, which, albeit also involves disagreement in the sign of the change among the ensemble members, still allows to conclude that no important changes are to be expected from these projections since all the ensemble members projects very slight changes.

Two facts contribute to the projected changes in Pmean: changes in the number of rainy days (ΔPF), and changes in the intensity of the precipitation in those rainy days (ΔPI). Figure 11 depicts their sign and their contribution. While the percentage of rainy days per season is projected to decrease in many sites in all seasons, droping 5–10 %, the intensity of the daily precipitation events is projected to increase. As seen above, the final result is a decrease in Pmean, but it is worth highlighting the opposite signs of these two contributions as it would indicate a tendency towards a precipitation regime with more uneven and intense events. Nonetheless, it should be stressed that spreads around 50 % of the *EM* projected changes emerge as well in these projections for PF and PI.

Contrary to the patterns of change for Pmean, the patterns of the ensemble mean-projected changes for precipitation variability (Figs. 9, 10m–p) depict the clearest

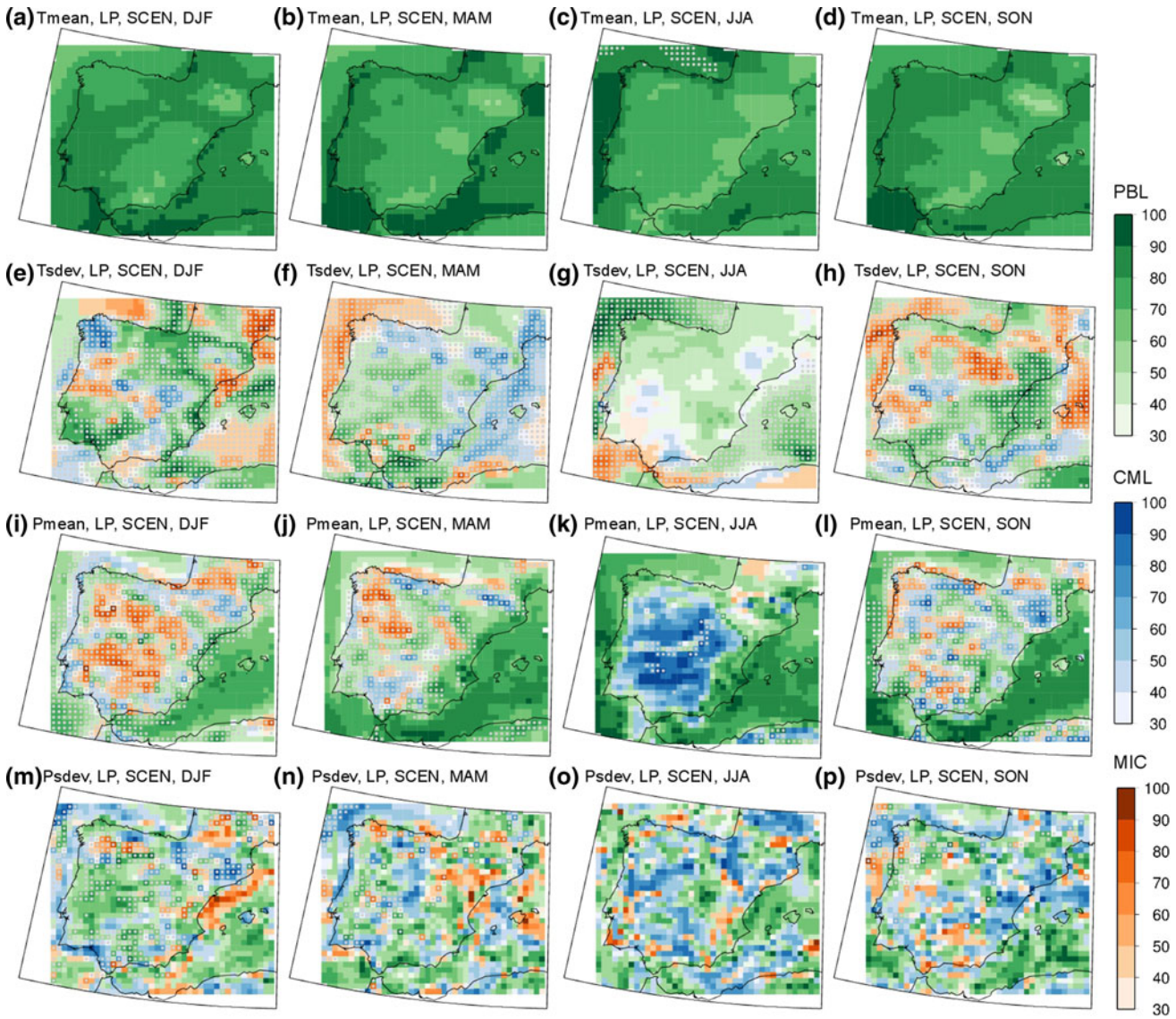

Fig. 7 As Fig. 4 but for the SCEN ensemble

signals in the winter season. These signals are overwhelmingly positive (30 mm/month, 70 %) with small discrepancies among the ensemble members. Thus, if Pmean is not projected to change severely but Psdev is clearly projected to increase, the conclusion arising is that the winter precipitation is projected to be more irregular in the future (i.e. dry winters followed by wet winters and vice versa). The *EM* change signals for Psdev in the rest of seasons are not statistically significant and the associated spread (20 % in spring, 40 % in autumn and 60 % in summer; with disagreement in the sign of the change in the great majority of cases) prevents from extracting clear conclusions.

This assessment further reveals the great sensitivity of the IP to future climate changes, yet highlighting the crucial role played by the model physics in the regional climate change projections supporting that statement. So much so that the reported spreads are of the same order as those obtained in multi-model ensembles (Table 2). In Table 2 the ensemble mean-projected changes and the associated spread after averaging for the whole IP for mean temperature and precipitation in the winter and summer seasons can be directly compared with those reported in Deque et al. (2007) based on a multi-model ensemble of similar projections for the same area and considering the same periods and emission scenario. Note that in the multi-model ensemble there is a mix of domain configurations and resolutions, nesting strategies, dynamic cores and physical configurations, all these factors contributing to the ensemble spread, while in our multi-physics single-model ensemble the spread is only attributable to the physical configuration of the regional model. Hence, the similar

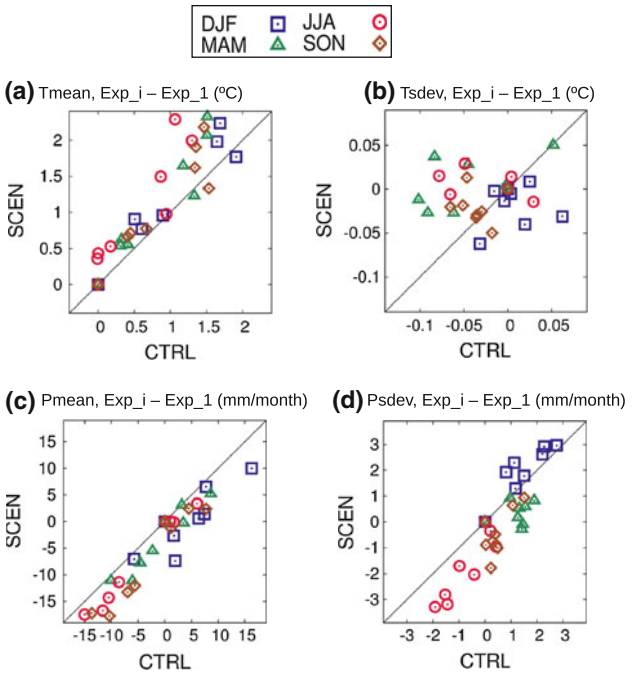

Fig. 8 As Fig. 5 but comparing CTRL and SCEN simulations

magnitude of the spreads obtained in both cases suggests that a large part of the multi-model spread could derive from the fact that the different models employ different physics.

6.2 Leading parameterized processes

This Section focuses on the leading parameterized processes for the projected changes. Previous Sections dealt with the *LPs* in the simulation of the climatology of the present or future periods, showing a great agreement in both cases except for Tsdev. However, Fig. 12 shows that the *LPs* for the future projections change. The unquestionable decisive role played by the PBL scheme for the simulation of the Tmean patterns in both present and future periods is dwarfed for the Tmean projections, while the negligible role of the MIC scheme pointed out in the previous Sections prevails now over the water mass areas (where, however, small spread appears) and everywhere in autumn (Fig. 12a–d). Changes in the *LPs* for the spread in ΔPmean compared to the *LPs* for the spread in Pmean are also observed. The CML scheme gains importance offshore, while in summer, inland, we now obtain a mixture of *LPs* in contrast with the clear signals of the previous assessments (Fig. 12i–l). The mixture remains in the case of ΔPsdev, but also depicting a different picture than before (Fig. 12m–p). Therefore, although some parameterized processes might not seem to be relevant when simulating the climatologies of a given period, they largely influence the result of future projections.

These changes of the *LPs* further implies that the order observed in Figs. 5, 8a, c, d disappears now when comparing the CTRL spatially averaged climatologies to the spatially averaged projected changes (Fig. 13a, c, d). In other words, there is no relationship between present-period biases and future projections within our ensemble. Therefore, although the warmest (for instance) configurations in the present period are still the warmest configurations in the future period, they are not those projecting the largest warming, likely because of the partial cancellation of errors when subtracting future minus present climatologies [the reader is here referred to an interesting dissertation about errors propagation and cancellation by Liang et al. (2008)]. However, given the important spreads accompanying the change signals, the cancellation of errors works only partially, mainly contributing to the change in the *LPs* aforementioned and to the disorder of Fig. 13a, c, d, being not enough to cancel the spread.

A different picture arises again in the case of ΔTsdev, which hence deserves a more detailed description. First we observe that the *LPs* for ΔTsdev (Fig. 12e–h) do resemble those for the simulated Tsdev in the present period (Fig. 4e–h). Second, that the magnitude of the projected changes depends on the simulated Tsdev in the present period, i.e. the larger Tsdev in the present period is, the smaller ΔTsdev is (Fig. 13b). Both features were actually expected since small spreads appeared in the SCEN ensemble regarding Tsdev, with all the simulations given similar results. Therefore, (1) discrepancies in the change signals derive from the discrepancies in the simulated Tsdev in the present period rather than from the discrepancies in the simulated Tsdev in the future period, and (2) the *LPs* for the spread in ΔTsdev are the *LPs* for the spread in the simulated Tsdev in the present period.

As discussed above, a possible explanation underlying this latter feature could be that the extremely dry conditions (in terms of soil moisture) dominating in the future scenario and constituting a constant boundary condition in terms of temperature variability, would force all the simulations to provide similar values of Tsdev in the SCEN ensemble, leaving them no space to develop distinct climatologies. The results in Jerez et al. (2012a) could indicate that the soil moisture availability acts as an upper limiting factor for the temperature variability over very dry soils (as occurring in the SCEN simulations). On the contrary, the soil moisture regime in the present period oscillating between wet and dry conditions allows for more freedom, namely spread, since depending on how the various physical parameterizations influence the simulation of the soil moisture content and handle its contribution, the result would vary dramatically. It is known that the role of the soil moisture is most important in summer, when the local circulation gains relevance in comparison to the

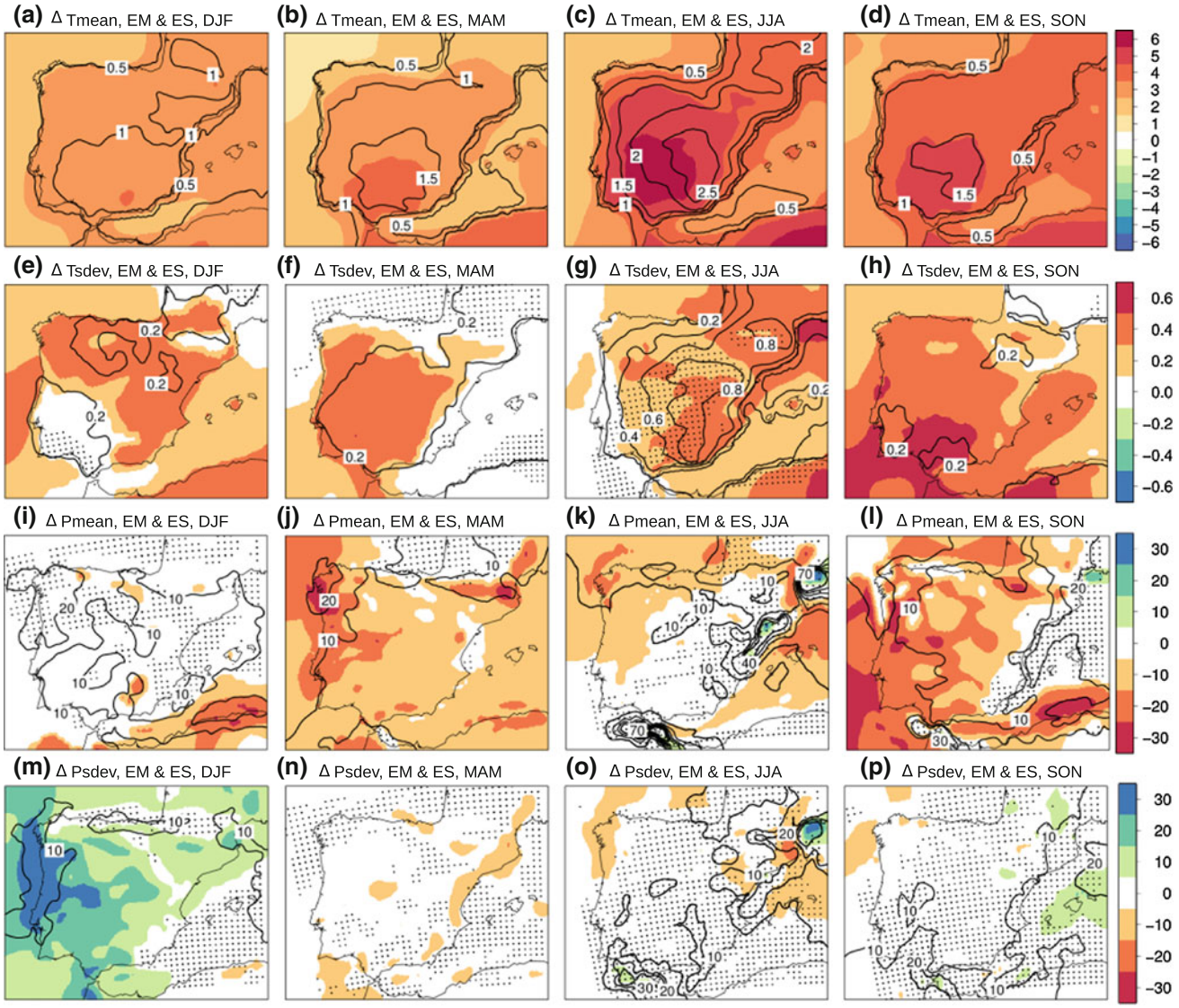

Fig. 9 Ensemble mean (*EM*) projected changes (SCEN minus CTRL climatologies; *shaded*) and the corresponding ensemble spread (*ES*) (contours) for Tmean (*first row*), Tsdev (*second row*), Pmean (*third row*) and Psdev (*fourth row*). Changes (from the *EM*) are displayed only if they are statistically significant at the 95 % confidence level. Each column, from *left* to *right*, represents the winter, spring, summer and autumn seasons. The *black dots* denote disagreement in the change sign between the various ensemble members. Units: K for temperature, and mm/month for precipitation

large-scale advective phenomena in the IP (Jerez et al. 2010). Hence, the most important spreads in ΔTsdev appear in the summer season (Fig. 12e–h), when, moreover, the *LPs* for the spread in both Tsdev and Pmean (the main source of soil moisture) in the present period are very coincident (Fig. 4g, k). Furthermore, it was previously mentioned that the disagreement in ΔTXsdev for the summer season among the various experiments is larger than in ΔTNsdev, and the larger influence of the soil moisture on the simulation of TX than of TN is also known (Jerez et al. 2012a). These features, although not strongly conclusive, reflect the plausibility of the proposed explanation.

More straightforward and expectable from previous works (Jerez et al. 2012a), soil moisture was found to underlay also regarding the obtained results for ΔTmean. The reasoning is as follows. The drier the soil is, the warmer the near-surface air temperature is, at least in the southern half of the IP in summer (Jerez et al. 2010, 2012a). In our ensemble both features also concur: the driest and warmest simulations coincide within both present and future periods along the ensemble (not shown), and are the same in both periods (Fig. 8a; not shown regarding soil moisture). Hence, the larger the projected depletion in soil moisture is, the higher the projected warming should be. This relationship is effectively observed in our experiments. Further, no proportionality has been found

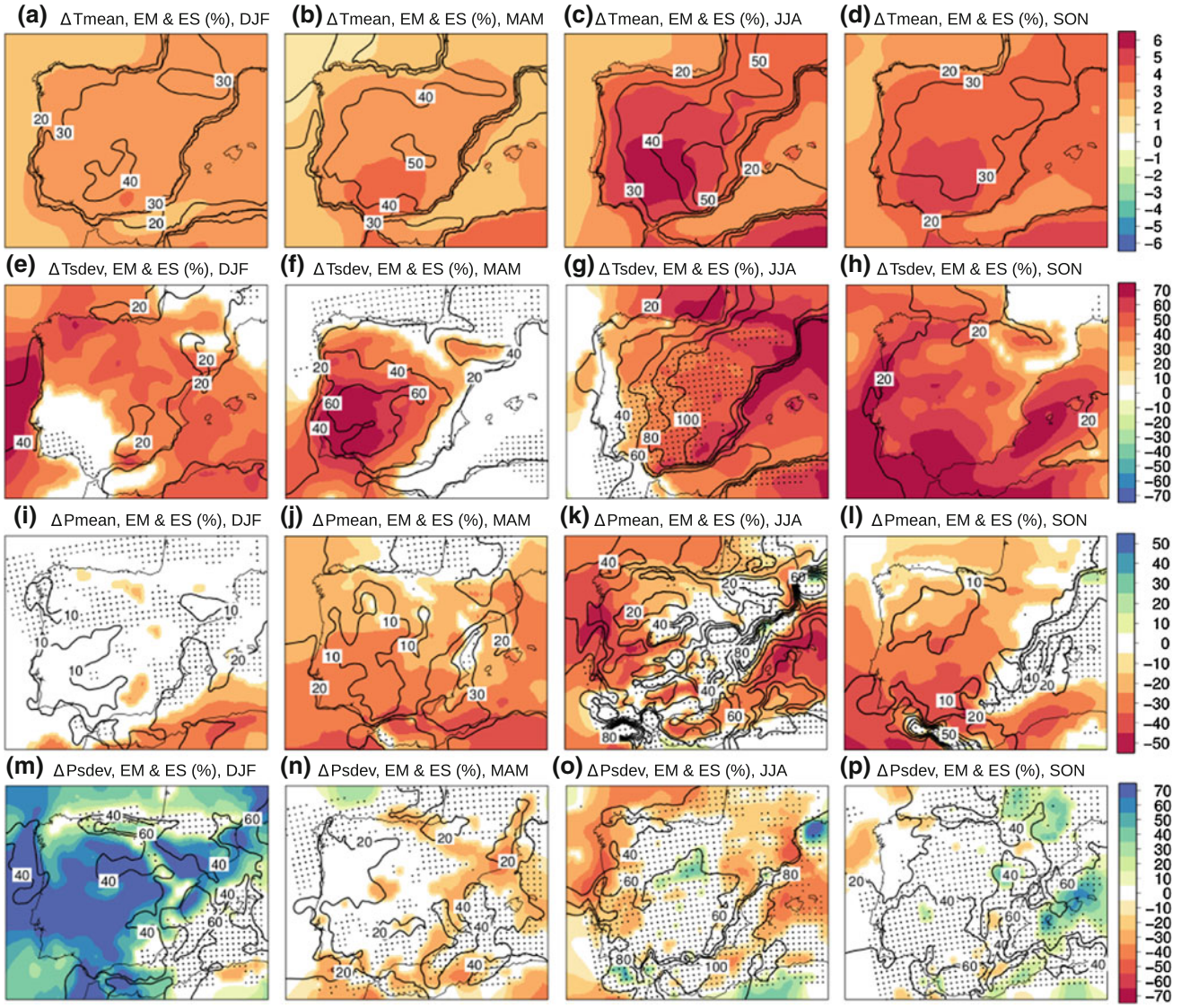

Fig. 10 Ensemble mean (*EM*) projected changes expressed in percentage with respect to the CTRL climatologies (i.e. [SCEN-CTRL/CTRL]·100) (*shaded*) and the corresponding ensemble spread (*ES*) obtained when changes are computed in percentage for each ensemble member (contours). Units: %. However, in the case of ΔTmean (*first row*) the *EM* projected change is given in K (as in Fig. 9) and the *ES* is given in percentage with respect to the ensemble mean projected change (i.e. $[ES/EM] \cdot 100$). Changes (from the *EM*) are displayed only if they are statistically significant at the 95 % confidence level. Each column, from *left* to *right*, represents the winter, spring, summer and autumn seasons. The *black dots* denote disagreement in the change sign between the various ensemble members

between the soil moisture content in the present period and the projected depletion of soil moisture, as no proportionality was found between present-day biases in mean temperature and the projected warming (Fig. 13a). Thus, these results reassert the close relationship between soil moisture and near-surface air temperature already established in the above referred studies.

7 Summary and conclusions

This work provides an assessment of the role of the model physics for regional climate change projections as a continuation of the previous work by Jerez et al. (2012b) highlighting the role of the model physics for regional present-day climate simulations. It reports on a multi-physics single-model ensemble of 30-year long simulations for the Iberian Peninsula (IP), a region that has been identified as a hot-spot area regarding climate change (Giorgi 2006), spanning both, a control (CTRL) reference period (1970–1999) and a future A2-scenario (SCEN) period (2070–2099). All the simulations were identically performed with a climate version of the mesoscale model MM5, just varying the physical options for modeling the planetary boundary layer (PBL), cumulus (CML) and

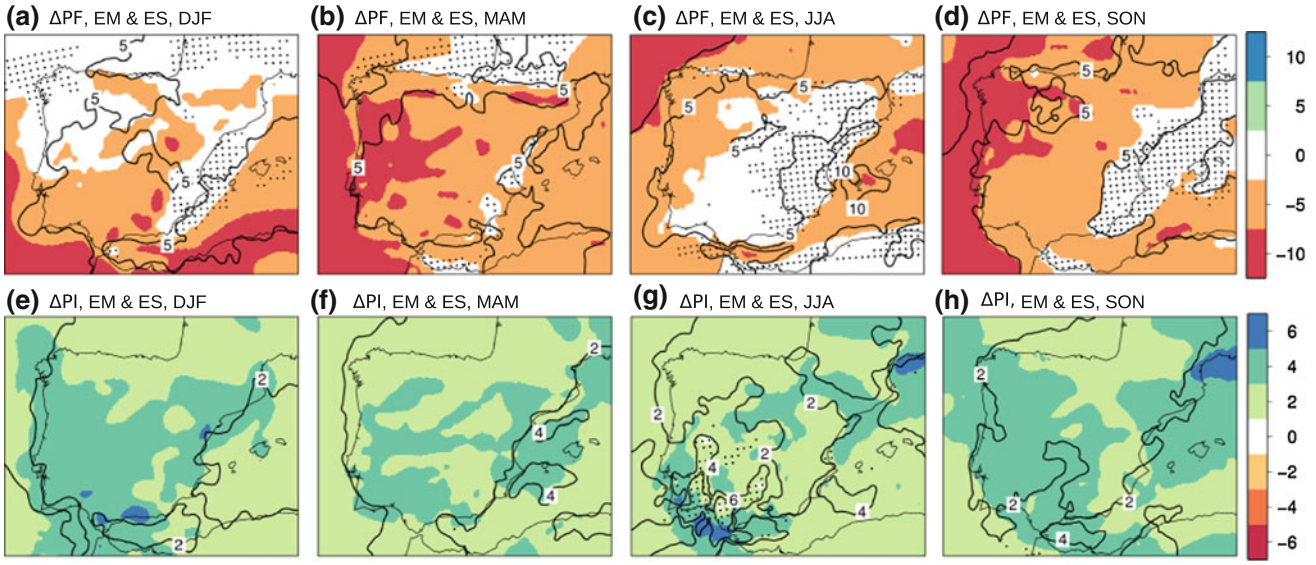

Fig. 11 Ensemble mean (*EM*) projected changes (SCEN minus CTRL climatologies; *shaded*) and the corresponding ensemble spread (*ES*) (contours) for frequency (PF, *first row*) and intensity (PI, *second row*) of the precipitation events. Changes (from the *EM*) are displayed only if they are statistically significant at the 95 % confidence level. Each column, from *left* to *right*, represents the winter, spring, summer and autumn seasons. The *black dots* denote disagreement in the change sign between the various ensemble members. Units: % for PF, and mm/day for PI

Table 2 Ensemble mean-projected changes (*EM*) and associated spread (*ES*) after averaging for the whole IP (land points) for mean temperature (T) and precipitation (P) in winter (DJF) and summer (JJA). *MS* denotes the multi-model spread reported in Deque et al (2007) for the same area and considering the same periods and emission scenario. Units: K for T and mm/month for P

	ΔTmean DJF	ΔTmean JJA	ΔPmean DJF	ΔPmean JJA
EM	3.0	4.6	−7.8	−5.6
ES	1.0	1.8	9.2	3.7
MS	1.7	3.5	0.9	20.1

microphysic (MIC) processes. Two options, among those offered by MM5, were considered in each case, resulting in an eight-member ensemble of CTRL simulations, SCEN simulations, and, thereby, climate change projections (i.e. SCEN minus CTRL). As in Jerez et al. (2012b), the analysis mainly focuses on mean values and standard deviations of the 2-m temperature (T) and precipitation (P) seasonal series; and uses typical estimates in the framework of ensembles (e.g. Deque et al. 2007; Jacob et al. 2007), such as the ensemble mean (*EM*) and the ensemble spread (*ES*).

The simulations were driven by the ECHAM5-Run1 global simulation. First, we provided a validation of this global database for the concrete purpose of simulating the IP climate at regional scales by comparison of the CTRL simulations with analogous hincasted (HNDC) simulations (Jerez et al. 2012b). Obtained GCM-induced errors mainly involve cold bias and underestimation of the interannual variability of the temperature series, and overprediction/underprediction of the heavy/light rainfall, yet providing an acceptable frame for the purpose of this study.

The comparison between the CTRL and the HNDC simulations also reveals that there are many areas showing both large biases and large spreads. This overlap suggests (1) the ability of the parameterized processes to modify the synoptic circulation, and (2) the dependence of the performance of the various parameterization schemes on the synoptic forcing. With respect to this latter, it has been explicitly shown that the *ES* patterns are notably different when comparing the CTRL and the HNDC ensembles or the CTRL and the SCEN ensembles. In particular, there is an overall intensification of the spreads under the future scenario.

Regardless of the driving conditions used, some invariant behaviors within the three ensembles (HNDC, CTRL and SCEN) have been identified. The so-called leading parameterized processes (*LPs*) for each variable, site and season are almost always the same. The PBL is the *LP* for simulating Tmean as the change of the PBL scheme contributes most to the *ES* in comparison to the changes of either the CML or the MIC scheme within our experimental design. As well, the CML is the *LP* mainly for simulating Pmean in the summer season. Although in other cases, the patterns displaying the *LPs* are quite mixed, such a mixture persists also similarly in the three ensembles. Furthermore, focusing on the individual ensemble members instead of on the averaged performance of the various schemes, we also obtain that the warmest (for instance)

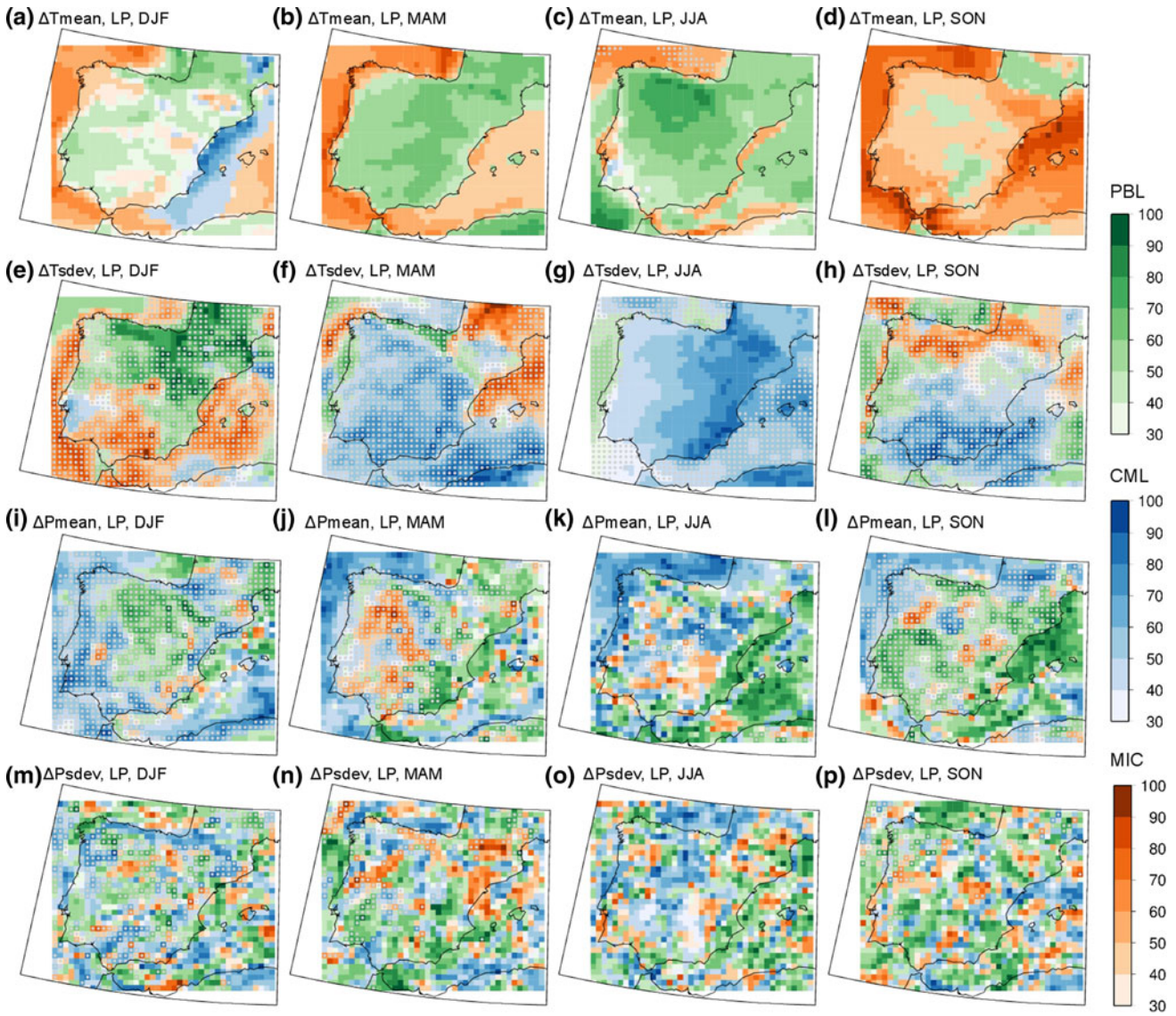

Fig. 12 Leading parameterized processes (*LPs*) for the simulated ΔTmean (*first row*), ΔTsdev (*second row*), ΔPmean (*third row*) and ΔPsdev (*fourth row*). The color indicate the *LP*: PBL (*green*), CML (*blue*) or MIC (*orange*). The intensity of the color represents the percentage of the mean ensemble spread (*MES*) attributed to the *LP* (units: %). The *gray dots* blur the areas where the *ES* expressed in percentage (as in Fig. 10) is below 20 %. Each column, from *left* to *right*, represents the winter, spring, summer and autumn seasons

configurations in the HNDC ensemble are still the warmest in the CTRL and the SCEN ensembles. This holds also for the rainiest configurations or those simulating the highest values of Psdev.

However, there is an overall exception regarding Tsdev: spreads diminish in the future scenario, the *LPs* change from one ensemble to another (i.e. from CTRL to SCEN), and there is not a persistent order among the various ensemble members. This indicates that the processes controlling the simulated Tsdev in the present climate become irrelevant in the future, when all the simulations converge within a small range. An open hypothesis exposed in the text, recalling the results of Seneviratne et al. (2006), Jerez et al. (2010, 2012a), invokes the role of the soil moisture as the controlling factor under the present conditions and the limiting factor under the future scenario.

The *EM* future projections roughly agree with previous reports (Perez et al. 2010; Gomez-Navarro et al. 2010; Jerez et al. 2012a), although they seem somewhat conservative especially for mean temperature. Temperature and temperature variability are projected to increase (up to 6 K and 70 %, respectively). Precipitation is projected to decrease (by up to 40 %), mainly due to the decrease in the frequency of the rainy days (while an overall increase in the intensity of the precipitation in those rainy days is projected), although some (quite uncertain) positive signals

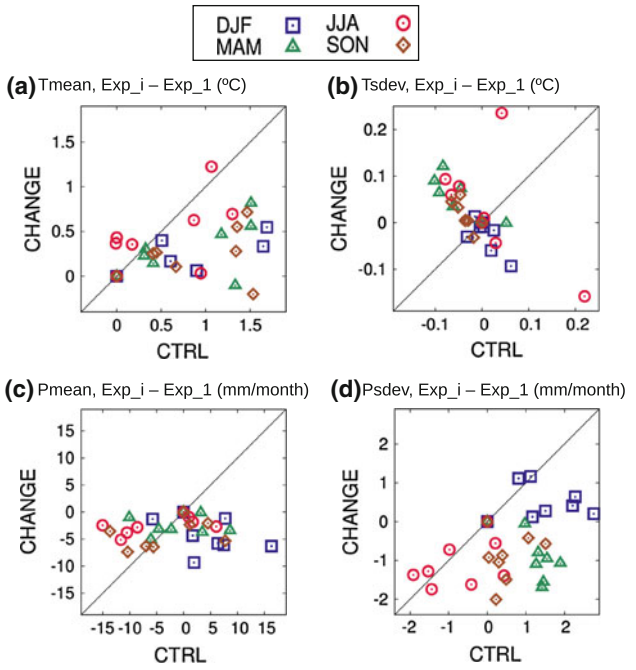

Fig. 13 As Figs. 5 and 8 but comparing CTRL simulations and changes (i.e. CTRL versus SCEN minus CTRL)

are found for small coastal areas of the eastern and southern IP. Precipitation variability is projected to increase (up to 70 %), pointing to qualitative changes in the precipitation regime towards more irregular and intense seasonal precipitation.

Large spreads accompany these *EM* signals of change. Spreads appear much more in the summer season, when they represent up to 50 % of the ensemble mean-projected change for mean temperature, up to 80 % in the case of mean precipitation, and above 100 % in the case of temperature and precipitation variability. They even involve disagreement between the ensemble members in the sign of the change except for mean temperature. The magnitude of these spreads is of the same order as the magnitude of the spreads obtained in multi-model ensembles (Deque et al. 2007), where not only the parameterization schemes but also a mixture of domain configurations, nesting strategies, resolutions, dynamic cores, etc. contributes to the obtained differences between the ensemble members. This may be an argument for stating that a large part of the inter-model spreads are related to the different physical parameterizations employed by the various models.

Finally, it has been shown that the *LPs* for simulating the climatology of a given period are not the same as the *LPs* when projecting future changes. While some processes could deserve little attention in the former case (at least the way in which they are modeled), their influence grows in the latter case, and vice versa. Hence, the cancellation of errors (Liang et al. 2008) works, although only partially (otherwise no spreads would appear in the ensemble of climate change projections), as it is further demonstrated by the fact that there is no proportionality between the climatologies in the present period and the projected changes (i.e. the warmest configurations are not those projecting the largest warming, for instance). However, the physical configurations reproducing the highest values of Tsdev in the present period do project the lowest increases (even decreases) of Tsdev for the future, i.e. all the simulations disagreeing under the present conditions tend, in the future, to the same aforementioned 'limit'.

These results deepen our knowledge about the key role of the parameterization schemes, particularly within regional climate models and for climate change applications. We feel that at the current state-of-the-science and in view of the results of works such as Fernandez et al. (2007), Argüeso et al. (2011), Jerez et al. (2012b) the reported spreads could be considered as a matter of uncertainty in the mean signals of change displayed here. Hence, further efforts to better understand and model the related sub-grid processes and their interactions with the large-scale phenomena are strongly encouraged.

Acknowledgments This work was funded by the Spanish Ministry of the Environment (Project ESCENA, Ref. 200800050084265) and the Projects CORWES (CGL2010-22158-C02-02) and SPEQ-TRES (CGL2011-29672-C02-02). The authors also gratefully acknowledge the funding from the Euro-Mediterranean Institute of Water Foundation (F-IEA). Pedro Jiménez-Guerrero acknowledges the Ramón y Cajal Programme. Sonia Jerez thanks the Portuguese Science Foundation (FCT) for her current financial support through the project ENAC (PTDC/AAC-CLI/103567/2008), and Ricardo M. Trigo for his personal scientific support.

References

Argüeso D, Hidalgo-Muñoz JM, Gámiz-Fortis SR, Esteban-Parra MJ, Dudhia J, Castro-Díez Y (2011) Evaluation of WRF parameterizations for climate studies over Southern Spain using a multistep regionalization. J Clim 24(21):5633–5651

Chen F, Dudhia J (2001) Coupling an advanced land surfacehydrology model with the Penn StateNCAR MM5 modeling system. Part I: model implementation and sensitivity. Mon Weather Rev 129(4):569–585

Christensen JH, Machenhauer B, Jones RG, Schär C, Ruti PM, Castro M, Visconti G (1997) Validation of present-day climate simulations over Europe: LAM simulations with observed boundary conditions. Clim Dyn 13:489–506

Christensen OB (1999) Relaxation of soil variables in a regional climate model. Tellus A 51(5):674–685

Deque M, Rowell DP, Lüthi D, Giorgi F, Christensen JH, Rockel B, Jacob D, Kjellstrm E, Castro MD, van den Hurk B (2007) An intercomparison of regional climate simulations for Europe: assessing uncertainties in model projections. Clim Change 81:53–70

Dudhia J (1989) Numerical study of convection observed during the winter monsoon experiment using a mesoscale two-dimensional model. J Atmos Sci 46(20):3077–3107

Evans JP (2008) Changes in water vapor transport and the production of precipitation in the eastern fertile crescent as a result of global warming. J Hydrometeorol 9(6):1390–1401

Evans JP (2010) Global warming impact on the dominant precipitation processes in the Middle East. Theoret Appl Climatol 99(3–4):389–402

Evans JP, Smith RB, Oglesby RJ (2004) Middle East climate simulation and dominant precipitation processes. Int J Climatol 24(13):1671–1694

Evans JP, Ekström M, Ji F (2012) Evaluating the performance of a WRF physics ensemble over South-East Australia. Clim Dyn. doi:10.1007/s00382-011-1244-5

Fernandez J, Montavez JP, Saenz J, Gonzalez-Rouco JF, Zorita E (2007) Sensitivity of the MM5 mesoscale model to physical parameterizations for regional climate studies: annual cycle. J Geophys Res 112:D04,101

Font-Tullot I (2000) Climatología de España y Portugal. Ed Universidad de Salamanca

Galos B, Lorenz P, Jacob D (2007) Will dry events occur more often in Hungary in the future? Environ Res Lett 2(3):034,006

Gianotti RL, Zhang D, Eltahir EAB (2012) Assessment of the regional climate model version 3 over the maritime continent using different cumulus parameterization and land surface schemes. J Clim 25(2):638–656

Giorgi F (2006) Climate change hot-spots. Geophys Res Lett 33:L08,707

Giorgi F, Bi X (2000) A study of internal variability of a regional climate model. J Geophys Res 105(D24):29503–29529

Gomez-Navarro JJ, Montavez JP, Jimenez-Guerrero P, Jerez S, Garcia-Valero JA, Gonzalez-Rouco JF (2010) Warming patterns in regional climate change projections over the Iberian Peninsula. Meteorol Z 19(3):275–285

Gomez-Navarro JJ, Montavez JP, Jerez S, Jimenez-Guerrero P, Lorente-Plazas R, Gonzalez-Rouco JF, Zorita E (2011) A regional simulation over the Iberian Peninsula for the last millenium. Clim Past 7(2):451–472

Gomez-Navarro JJ, Montavez JP, Jimenez-Guerrero P, Jerez S, Lorente-Plazas R, Gonzalez-Rouco JF, Zorita E (2012) Internal and external variability in regional simulations of the Iberian Peninsula climate over the last millennium. Clim Past 8:25–36

Grell GA (1993) Prognostic evaluation of assumptions used by cumulus parameterizations. Mon Weather Rev 121(3):764–787

Grell GA, Dudhia J, Stauffer DR (1994) A description of the fifth-generation Penn State/NCAR Mesoscale Model (MM5). NCAR Tech Note 398+STR, Natl Cent for Atmos Res, Boulder, CO

Han Z, Hiromasa U, An J (2008) Evaluation and intercomparison of meteorological predictions by five MM5-PBL parameterizations in combination with three land-surface models. Atmos Environ 42(2):233–249

Haugen JE, Iversen T (2008) Response in extremes of daily precipitation and wind from a downscaled multi-model ensemble of anthropogenic global climate change scenarios. Tellus A 60(3):411–426

Herrera S, Fita L, Fernandez J, Gutierrez JM (2010) Evaluation of the mean and extreme precipitation regimes from the ENSEMBLES regional climate multimodel simulations over Spain. J Geophys Res 115:D21

Hong SY, Pan HL (1996) Nonlocal Boundary Layer vertical diffusion in a medium-range forecast model. Mon Weat Rev 124:2322–2339

IPCC (2007) Summary for policymakers. In: Solomon S, Qin D, Manning M, Chen Z, Marquis M, Averyt KB, Tignor M, Miller HL (eds) Climate change 2007: the physical science basis. Contribution of working group I to the fourth assessment report of the intergovernmental panel on climate change, Cambridge University Press, Cambridge, UK

Jacob D, Barring L, Christensen OB, Christensen JH, de Castro M, Deque M, Giorgi F, Hagemann S, Lenderink G, Rockel B, Sanchez E, Schaer C, Seneviratne SI, Somot S, van Ulden A, van denHurk B (2007) An inter-comparison of regional climate models for Europe: model performance in present-day climate. Clim Change 81:31–52

Janjic ZI (1994) The step-mountain eta coordinate model: further developments of the convection, viscous sublayer, and turbulence closure schemes. Mon Weather Rev 122(5):927–945

Jerez S, Montavez JP, Gimenez D (2009) Optimizing the execution of a parallel meteorology simulation code. IEEE international symposium on parallel and distributed processing (Rome, 2009) pp 1–6

Jerez S, Montavez JP, Gomez-Navarro JJ, Jimenez-Guerrero P, Jimenez J, Gonzalez-Rouco JF (2010) Temperature sensitivity to the land-surface model in MM5 climate simulations over the Iberian Peninsula. Meteorol Z 19(4):363–374

Jerez S, Montavez JP, Gomez-Navarro JJ, Jimenez PA, Jimenez-Guerrero P, Lorente-Plazas R, Gonzalez-Rouco JF (2012a) The role of the land-surface model for climate change projections over the Iberian Peninsula. J Geophys Res 117:D01,109

Jerez S, Montavez JP, Jimenez-Guerrero P, Gomez-Navarro JJ, Lorente-Plazas R, Zorita E (2012b) A multi-physics ensemble of present-day climate regional simulations over the Iberian Peninsula. Clim Dyn. doi:10.1007/s00382-012-1539-1

Joshi M, Hawkins E, Sutton R, Lowe J, Frame D (2011) Projections of when temperature change will exceed 2 C above pre-industrial levels. Nature Clim Change 1(8):407–412

Jung G, Kunstmann H (2007) High-resolution regional climate modeling for the Volta region of West Africa. J Geophys Res (Atmospheres) 112(11):D23,108

Kain JS, Fritsch JM (1990) A one-dimensional entraining/detraining plume model and its application in convective parameterization. J Atmos Sci 47(23):2784–2802

Kanamitsu M, Ebisuzaki W, Woollen J, Yang SK, Hnilo JJ, Fiorino M, Potter GL (2002) NCEP-DOE AMIP-II reanalysis (R-2). Bull Am Meteorol Soc 83:1631–1643

Knutson TR, Tuleya RE (2004) Impact of CO2-induced warming on simulated hurricane intensity and precipitation: sensitivity to the choice of climate model and convective parameterization. J Clim 17(18):3477–3495

Koo GS, Boo KO, Kwon WT (2009) Projection of temperature over Korea using an MM5 regional climate simulation. Clim Res 40(2–3):241–248

Leander R, Buishand TA (2007) Resampling of regional climate model output for the simulation of extreme river flows. J Hydrol 332(3–4):487–496

Leung LR, Gustafson WI (2005) Potential regional climate change and implications to US air quality. Geophys Res Lett 32:L16,711

Liang XZ, Kunkel KE, Meehl GA, Jones RG, Wang JXL (2008) Regional climate models downscaling analysis of general circulation models present climate biases propagation into future change projections. Geophys Res Lett 35(8):L08,709

Lo JCF, Yang ZL, Pielke RA (2008) Assessment of three dynamical climate downscaling methods using the Weather Research and Forecasting (WRF) model. J Geophys Res 113:D09,112

Mlawer EJ, Taubman SJ, Brown PD, Iacono MJ, Clough SA (1997) Radiative transfer for inhomogeneous atmospheres: RRTM, a validated correlated-k model for the longwave. J Geophys Res 102:16663–16682

Nakicenovic N, Alcamo J, Davis G, de Vries B, Fenhann J, Gaffin S, Gregory K, Grübler A, Jung TY, Kram T, La Rovere EL, Michaelis L, Mori S, Morita T, Pepper W, Pitcher H, Price L, Raihi K, Roehrl A, Rogner HH, Sankovski A, Schlesinger M, Shukla P, Smith S, Swart R, van Rooijen S, Victor N, Dadi Z

(2000) IPCC special report on emissions scenarios, Cambridge University Press, Cambridge

Perez FF, Boscolo R, Blade I, Cacho I, Castro-Diez Y, Gomis D, Samperiz G, Miguez-Macho G, Rodriguez-Fonseca B, Rodriguez-Puebla C, et al. (2010) Clima en España: pasado, presente y futuro. Informe de Evaluacion del Cambio Climatico Regional

Ratnam JV, Kumar KK (2005) Sensitivity of the simulated monsoons of 1987 and 1988 to convective parameterization schemes in MM5. J Clim 18(14):2724–2743

Reisner J, Rasmussen RM, Bruintjes RT (1998) Explicit forecasting of supercooled liquid water in winter storms using the MM5 mesoscale model. Quart J R Meteorol Soc 124(548):1071–1107

Roeckner E, Bäuml G, Bonaventura L, Brokopf R, Esch M, Giorgetta M, Hagemann S, Kirchner I, Kornblueh L, Manzini E, Rhodin A, Schlese U, Schulzweida U, Tompkins A (2003) The atmospheric general circulation model ECHAM 5. PART I: model description. Max-Planck-Institute for Meteorology

Rummukainen R (2010) State-of-the-art with regional climate models. WIREs Clim Change 1:82–96

Salzmann N, Frei C, Vidale P, Hoelzle M (2007) The application of Regional Climate Model output for the simulation of high-mountain permafrost scenarios. Global Planet Change 56(1–2):188–202

Sanchez E, Gallardo C, Gaertner MA, Arribas A, Castro M (2004) Future climate extreme events in the Mediterranean simulated by a regional climate model: a first approach. Global Planet Change 44(1–4):163–180

Seneviratne SI, Lüthi D, Litschi M, Schär C (2006) Land-atmosphere coupling and climate change in Europe. Nature 443(7108): 205–209

Snedecor GW, Cochran WG (1989) Statistical methods, 8th edn. Iowa State University Press, Oxford

Soares PMM, Cardoso RM, Miranda PMA, Viterbo P, Belo-Pereira M (2012) Assessment of the ENSEMBLES regional climate models in the representation of precipitation variability and extremes over Portugal. J Geophys Res 117:D7

Stensrud D (2007) Parameterization schemes: keys to understanding numerical weather prediction models. Cambridge University Press, Cambridge

Tebaldi C, Knutti R (2007) The use of the multi-model ensemble in probabilistic climate projections. Philos Trans R Soc A Math Phys Eng Sci 365(1857):2053–2075